# A high-resilience and conductive composite binder for lithium-sulfur batteries

# A high-resilience and conductive composite binder for lithium-sulfur batteries

**Mengyao Zheng[a,1], Xiaomin Cai[a,1] Yafang Tan[a], Wenqiang Wang[a], Dongya Wang[a], Haojie Fei[b], Petr Saha[b], Gengchao Wang[a*]**

[a]*Shanghai Key Laboratory of Advanced Polymeric Materials, Shanghai Engineering Research Center of Hierarchical Nanomaterials, School of Materials Science and Engineering, East China University of Science and Technology, P.O. Box 289, 130 Meilong Rd., Shanghai 200237, PR China*

[b]*Centre of Polymer Systems, University Institute, Tomas Bata University, Tř. T. Bati 5678, Zlin-76001 Zlín, Czech Republic*

** Corresponding author. E-mail address: gengchaow@ecust.edu.cn (G. Wang). 1 These authors contributed equally.*

**HIGHLIGHTS**

- The WPU/PAA/graphene multi-functional composite binder was fabricated.
- Physical crosslinking of multiple hydrogen bonds to achieve high resilience.
- Well-dispersed graphene provides electronic channels and large area reactive sites.
- Active resilience adapts to the volume change of sulfur cathode.
- The Li-S batteries based on WPU/PAA/graphene binder show excellent cycle stability.

**ABSTRACT**

Binder is very important for the cycle stability of lithium-sulfur batteries under high sulfur loading. In this paper, we designed and prepared a waterborne polyurethane/polyacrylic acid/graphene (WPU/PAA/GN) multi-functional composite binder. The polyoxyethylene segments in WPU are used to promote the migration of lithium ions and provide high elongation. The introduction of polyacrylic acid (PAA) and graphene forms a double hydrogen bond network through simple in situ blending, which gives the binder higher strength and electronic conductivity. More importantly, the physical crosslinking of PAA and WPU can achieve high resilience and ensure the integrity of the cathode structure during charging and discharging. In addition, abundant polar functional groups provide strong chemical adsorption for lithium polysulfide. The synergistic effect of various components makes the binder possess the functions of high resilience, good electrical conductivity, and strong adsorption, which provides a simple and effective solution for the practical application of lithium-sulfur batteries. As a result, the assembled lithium-sulfur battery displayed a high initial discharge capacity of 1243 mAh $g^{-1}$, good cycle stability (81% capacity retention after 500 cycles at 0.5 C) and superior rate performance.

*Keywords*: Conductive binder Dynamic cross-linking Polysulfides adsorption Sulfur cathodes

## 1. Introduction

The ever-increasing demand for portable electronics, electric vehicles and grid applications has inspired the development of advanced energy storage systems **[1-4].** In this regard, lithium-sulfur (Li-S) batteries, as the next generation of high energy rechargeable batteries, have been paid much attention due to their high theoretical capacity (1675 mAh g-1) and high energy density (2600 Wh $Kg^{-1}$) **[5-12]**. In addition, elemental sulfur is a promising cathode material, which is low-cost, abundant and environment-friendly **[13-15]**. Nevertheless, the commercial application of Li-S batteries is hindered by a series of problems, such as the insulating nature of sulfur and lithium polysulfides (LiPSs), the dissolution and shuttle effect of LiPSs in the liquid electrolyte, volume expansion and shrink of sulfur during discharge-charge process **[16-23]**.

In recent years, researchers have developed high-sulfur loading cathodes to match the energy density required for practical application of Li-S batteries **[24-28]**. However, with the increase of sulfur loading, the film of electrodes coated on the collector will become thicker. After drying, the thick electrodes tend to break down and separate from the collector, which makes it difficult to achieve electrochemical stability under high sulfur loading **[29-31]**.

Although the total weight of binder in the electrode is less than 10%, it is very important to ensure the structural integrity of the electrode and alleviate the volume effect of active substances **[32-34]**. At present, commonly used binders such as PVDF and PAA have low elongation at break **[35-39]**. When the volume of the electrode expands or deforms during charging and discharging, inelastic binders will cause the particle powdering and the loss of electronic conductivity **[40,41]**. In addition, there is no bond between the binder and the intermediate product LiPSs and the rapid dissolution of LiPSs will cause the capacity to decay with time **[42-44].**

In order to solve these problems, researchers have done a lot of work to prepare functional binders. Firstly, the shuttle of LiPSs needs to introduce polar functional groups into the binder **[40,45,46]**. For example, Wahyudi et al. **[47]** prepared polyethersulfone binder, using its abundant sulfonyl group (O=S=O) as the active site, effectively reduced the loss of active substances by chemisorption combined with LiPSs. Secondly, high elasticity is essential to ensure the structural integrity of the electrodes during the cycling process **[45,48]**. Xu et al. **[49]** designed a kind of water binder with self-healing multiple-network structure. The design concept of both hard and soft endows the material with excellent tensile properties. Furthermore, conductive polymer/ carbon materials are introduced to give the binder electronic conductivity **[50-56]**. Milroy et al. **[57]** use highly conjugated polypyrrole to form an electro-osmosis network in the binder matrix, which provides a conductive path for insulator sulfur. Thus, it is obvious that the single-function binder cannot meet the needs of high sulfur loading and long cycling life of lithium-sulfur batteries **[58,59]**.

Herein, we prepared a waterborne polyurethane/polyacrylic acid/ graphene (WPU/PAA/GN) multi-functional composite binder. Among them, WPU is used as binder in lithium-sulfur batteries for the first time, because the polyether chain in its molecular chain can be used as a grasper to capture lithium ions and accelerate the migration of lithium ions. Polyacrylic acid (PAA), graphene and WPU were blended in situ to form a double hydrogen-bond network structure to further enhance the strength and resilience of the binder, thereby alleviating the volume change and electrolyte resistance of lithium sulfur batteries during charging and discharging. Abundant polar groups such as carbamate (-NHCOO-) and carboxyl (-COOH) can achieve strong chemical capture of LiPSs and thus inhibit shuttle effect. More importantly, the formation of physical crosslinking network between WPU and PAA gives the binder high-elasticity, which is essential for the structural stability of the electrode. In addition, the introduction of graphene can greatly increase the electronic conductivity. As a result, compared with

batteries using PVDF and WPU-PAA binders, WPU-PAA-GN battery had higher specific capacity, better cycle stability and superior rate performance.

## 2. Experimental section

### *2.1. Preparation of waterborne polyurethane (WPU)*

First, 0.04 mol polyethylene glycol (PEG, Mn = 1000, Sinopharm Chemical Reagent Co., Ltd, China) was charged into a four-necked round bottom flask equipped with a thermometer and a mechanical stirrer. Vacuum dehydration was performed at 110 °C for 1 h, and then dimethylolpropionic acid (DMPA, Sinopharm Chemical Reagent Co., Ltd, China) with different contents (4.9 wt%, 6.7 wt%, and 8.6 wt%) was added to continue to remove water at 85 °C for 1.5 h. Next, N-methyl-2-pyrrolidone (NMP) and isophorone diisocyanate (IPDI, Sinopharm Chemical Reagent Co., Ltd, China) were added and reacted with PEG and DMPA under argon atmosphere at 80 °C for 1 h. The amount of IPDI is determined by the theoretical hydroxyl content (n(-NCO) = 1.6n(-OH)). Dibutyltin dilaurate (DBTDL) was added to accelerate the reaction at 80 °C for 1.5 h. After cooling to 60 °C, trie-thylamine (TEA) with the molar ratio of 1: 1 to DMPA to neutralize the DMPA for 0.5 h. The prepolymer was dispersed in deionized water under high-speed shearing, then 0.04 mol ethylenediamine (EDA) was added to the reactor and stirred at 40 °C for 2 h. Finally, waterborne polyurethane with a solid content of about 30 wt% was obtained. The specific synthesis process is shown in **Fig. S1**.

### *2.2. Preparation of well-dispersed graphene*

The well-dispersed GN was prepared through 60Co y-ray with irradiation doses of 100 kGy and the detailed process was shown in Supporting Information **[60]**.

### *2.3. Preparation of WPU-PAA and WPU-PAA-GN binders*

To prepare the WPU-PAA-GN binder, 0.06 g WPU was added into 1.2 mL N, N-dimethylacetamide/water (V:V, 1:1) and stirred 2 h to form a uniform dispersion, followed PAA ($M_W$ = 450,000) aqueous solution (solid content is 5 wt%) was added into the above solution with mechanical stirring at room temperature for 2 h. Among them, control the mass ratio of WPU: PAA = 9:1∼5:5, and then the WPU-PAA binder was obtained. Finally, GN with different contents (0.5 wt%, 1 wt %, and 1.5 wt%) was incorporated into the WPU-PAA solution with vigorous stirring for 12 h. The obtained composite binder was WPU-PAA-GN binder.

### *2.4. Preparation of sulfur cathode and assembly of battery*

The S/C composite is obtained by ball milling for 6 h and melting in an argon atmosphere at 155 °C for 12 h (S: Super P = 3:1). The electrodes were prepared by ball milling the S/C composite, conductive agent (MWCNT) and binder (PVDF, WPU-PAA, WPU-PAA-GN) in a mass ratio of 8:1:1 for 4 h. At the same time, the solid content of the slurry is controlled to 25 wt%. The obtained slurry was coated on aluminum foil and was put into vacuum oven for 12 h at 50 °C to dry. The area of cathode was 1.13 cm2, and the sulfur loading was 2.3 mg $cm^{-2}$.

Coin type (CR2016) cells were assembled in an argon filled glove box. The sulfur cathode was separated from the lithium anode with polypropylene film (Celgard 2400). The electrolyte consisted of 1 M lithium bis-(trifluoromethylsulfonyl) imide (LiTFSI) in the mixture of 1,2-dimethoxyethane and 1,3-DOL (1:1, V/V) containing $LiNO_3$ (1 wt %). In addition, the amount of electrolyte is determined by the mass of sulfur, which is 20 µL $mg^{-1}$.

### *2.5. Characterization and electrochemical measurements*

Morphologies of the samples were characterized with a field-emission scanning electron microscopy (FE-SEM, Hitachi S4800) and high-resolution transmission electron microscopy (HRTEM, JEOL JEM-2100). The Fourier transform infrared spectroscopy (FTIR) was obtained using a Nicolet 6700 spectrometer with a resolution of 2 $cm^{-1}$. Raman spectra were performed with a Renishaw via Raman spectrometer system. X-ray diffraction (XRD) was performed using a Rigaku D/ Max 2550 VB/PC X equipped with a Cu target X-ray tube. The thermal gravimetric analyses (TGA, NETZSCH TG209F1-GC) were carried out from room temperature to 600 °C at a heating rate of 10 °C $min^{-1}$ under Nitrogen atmosphere. Dynamic thermomechanical analysis (DMA) was recorded on TA DMA Q800. Differential scanning calorimetry (DSC) was performed on a modulated DSC2910 (USA). The tensile tests and cyclic tensile test were carried out at a strain rate of 50 mm $min^{-1}$ and 25 mm $min^{-1}$ using a Mark-10 testing machine.

Cyclic voltammetry (CV) and electrochemical impedance spectroscopy (EIS) was conducted with a CHI 660D electrochemical workstation. The galvanostatic charge-discharge profiles between 1.5 V and 3 V was performed by LAND CT2001A.

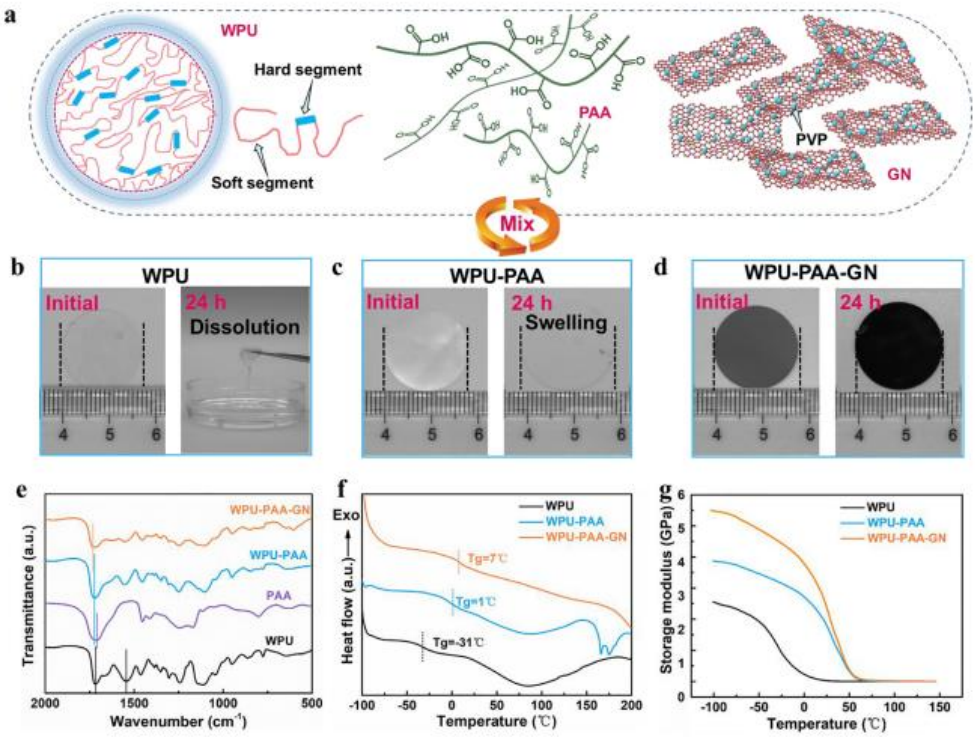


**Fig. 1.** (a) Schematic of the formation process of WPU-PAA-GN composite binder. Digital photos of (b) WPU, (c) WPU-PAA, and (d) WPU-PAA-GN membranes before and after soaking in DOL/DME for 24 h. (e) FTIR spectra, (f) DSC curves, and (g) Storage modulus of WPU, WPU-PAA, and WPU-PAA-GN.

## 3. Results and discussion

As shown in **Fig. 1**a, WPU-PAA-GN composite binder is composed of high elastic waterborne polyurethane (WPU), high-strength polyacrylic acid (PAA) and easily dispersed graphene (GN) by simple blending. Among them, WPU is the key matrix material to ensure high resilience. In order to optimize the composition of WPU, we investigated the effect of the amount of hydrophilic chain-extender dimethylolpropionic acid (DMPA) on the mechanical properties and ionic conductivity (**Fig. S2**a-**2**c). It was found that when DMPA content was 6.7 wt%, the comprehensive properties of WPU were the best, with breaking strength of 7.9 MPa, elongation at break of 863%, peel strength of 15.5 MPa, and ionic conductivity of 5.6 mS $cm^{-1}$ after absorbing electrolyte.

However, WPU is not resistant to electrolyte, as shown in **Fig. 1**b, after soaking in DOL/DME (1:1, V/V) solvent for 24 h, WPU film (DMPA-6.7 wt%) dissolved. In order to improve the solvent resistance of WPU, we introduce PAA which is rich in carboxyl group. It can realize physical crosslinking with WPU through multiple hydrogen bonds, and further enhance the strength of binder. In order to study the effect of PAA content on WPU, the mechanical properties were tested. It is found that with the increase of the rigid chain PAA, the tensile strength (**Fig. S3**a) and bond strength (**Fig. S3**b) of WPU-PAA film reaches the maximum at 6:4 of WPU/PAA mass ratio. However, when the WPU/PAA mass ratio increases to 5:5, the tensile strength and bonding ability are reduced, which is ascribed to the micro-phase separation between the WPU and the PAA **[61].** The Tg in DSC curves (**Fig. S3**c) shifts to the low temperature further proves this view. Therefore, the proportion of WPU/PAA = 6:4 was chosen for further study.

However, the introduction of PAA does not completely solve the dissolution problem of WPU, and slight swelling still occur in DOL/DME solvent (**Fig. 1**c), which is very unfavorable for the stability of electrode structure. Therefore, we introduce graphene into WPU-PAA, which not only enhances the electronic conductivity, but also improves the solvent resistance of the binder. After soaking in DOL/DME solvent for 24 h, almost no swelling occurs (**Fig. 1**d). In addition, gel fraction test (**Fig. S4**) further proves that WPU-PAA-GN has good electrolyte resistance. However, graphene is easy to agglomerate. In order to improve its dispersion in binder, a small amount of Polyvinylpyrrolidone (PVP) was added. High electronic conductivity (3.75 S $cm^{-1}$) and well-dispersed reduced graphene oxide/PVP (GN) were prepared by y-ray irradiation reduction technology. It can be seen from the FE-SEM image (**Fig. S5**a) that the GN displays a thin layer structure without serious stacking. After 30 days of storage, there is still no settlement (**Fig. S5**b). The influence of irradiation reduction on the chemical composition and structure of graphene can be further confirmed by XRD **(Fig. S5**c) and EDS (**Fig. S5**d). In **Fig. S5**c, there is a sharp diffraction peak at 8.8° for graphene oxide, representing its (0 0 1) crystal surface, and a wide diffraction peak near 25.8° for the reason of the random stacking between the layers of exfoliated graphene oxide. After PVP was added, the diffraction peak moved to the low angle direction, which was mainly due to the intercalation of PVP, resulting in the increase of graphene layer spacing. After irradiation reduction, the diffraction peak of graphene (0 0 1) crystal surface disappeared completely. In addition, the oxygen element in EDS spectrum (**Fig. S5**d) is obviously reduced, and the C/O mass ratio is increased from 1.8 to 5.1, which indicates that graphene is effectively produced by ϒ-ray irradiation. The addition of GN has a significant effect on the properties of WPU-PAA-GN film (**Fig. S6**a and **6**b). When the addition of GN is 1 wt%, the tensile strength, elongation at break and bond strength of WPU-PAA-GN are the highest. TEM images also showed that when the content of GN was 1 wt%, GN was uniformly dispersed in the polymer matrix (**Fig. S6**c), while when the content of GN was 1.5 wt%, there was some agglomeration (**Fig. S6**d). Therefore, the WPU-PAA-GN composite binder with 1 wt% GN was chosen as the further research object.

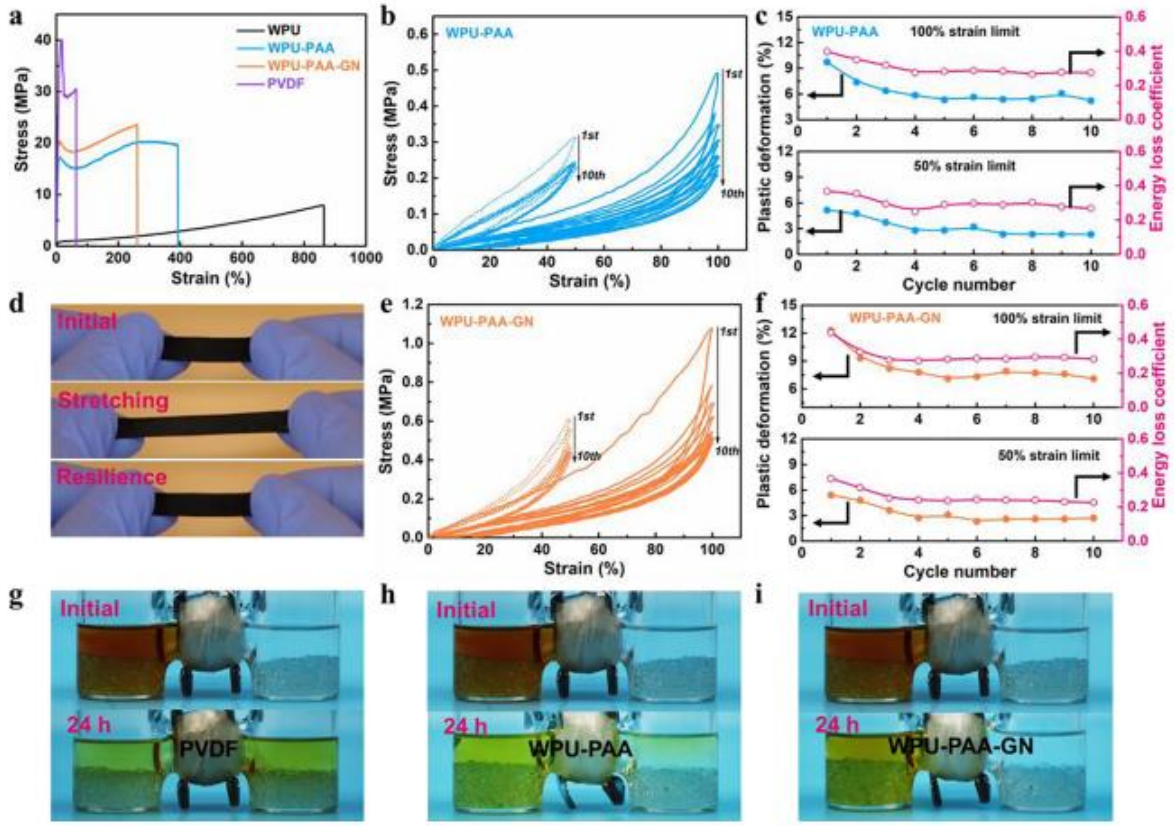


**Fig. 2.** (a) Stress-strain curves of WPU, WPU-PAA, WPU-PAA-GN and PVDF. (b) Stress-strain curves and (c) the corresponding plastic deformation/energy loss coefficient of WPU-PAA with 100% electrolyte uptake rate for 10 stretch-recovery cycles with different strain limits. (d) Digital photos of WPU-PAA-GN in initial/ stretching/resilience states. (e) Stress-strain curves and (f) the corresponding plastic deformation/energy loss coefficient of WPU-PAA-GN with 100% electrolyte uptake rate for 10 stretch-recovery cycles with different strain limits. The adsorption-barrier action tests of (g) PVDF, (h) WPU-PAA, (i) WPU-PAA-GN films between Li2S6 and DOL/DME solution.

In order to study the interaction among the WPU, the PAA and the GN, the FTIR spectra were measured (**Fig. 1e**). It was found that the characteristic peak of N-H appeared in WPU at 1540 $cm^{-1}$, and the characteristic peak of hydrogen-bonded C=O appeared at 1716 cm-1. The peak of the hydrogen-bonded C=O in PAA appeared at 1710 $cm^{-1}$. It was worth noting that when WPU and PAA were mixed, the C=O peak blue shifted to 1722 $cm^{-1}$. This is ascribed to the fact that the hydrogen bonds among the carbamate groups of WPU and the carboxyl groups of PAA change to that between the WPU and the PAA, which effectively inhibits the microphase separation between the WPU and PAA. Furthermore, with the addition of GN, the C=O peak blue shifts to 1727 $cm^{-1}$, indicating that the microphase separation between the WPU and PAA further inhibits. In addition, the DSC curves of **Fig. 1**f show that the glass transition temperature (Tg) gradually increases from - 31 °C of WPU to 1 °C of WPU-PAA binary system and 7 °C of WPU-PAA-GN ternary system, which also indicates that the three components have good compatibility after the addition of PAA and GN. In addition, from the dynamic thermomechanical analysis (DMA) curves **(Fig. 1**g), it can be seen that with the addition of PAA and GN, the storage modulus of the membrane increases gradually, which benefits from the good compatibility of the three components.

In order to study the ability of the binder to adapt to the volume change of the active material in the process of charging and discharging, we tested the stress-strain and resilience properties. **Fig. 2**a was

the stress-strain curves of WPU, WPU-PAA, WPU-PAA-GN and PVDF. With the addition of PAA, the tensile strength of WPU can be greatly improved from 7.7 to 19.7 MPa. Furthermore, with the addition of GN, the tensile strength was further increased to 23.6 MPa, and the elongation at break was still maintained at 261%. This was mainly due to the dual effects of physical crosslinking between WPU and PAA and the enhancement of GN. In order to further explain the interaction among the three components, we tested the stress-strain curves and electrolyte resistance of WPU-GN, PAA and PAA-GN. As shown in **Fig. S7**a and **S7**b, compared with the tensile strength (12 MPa) and the elongation at break (548%) of WPU-GN, the tensile strength of PAA and PAA-GN is further improved, but the elongation at break is very low. After soaking in the DOL/DME solvent for 24 h, WPU-GN had obvious swelling **(Fig. S7**c) while PAA and PAA-GN hardly changed (**Fig. S**7d and **S7**e). **Fig. 2**b and e showed the stretch-recovery curves of WPU-PAA and WPU-PAA-GN films with 100% absorption of electrolyte, respectively.

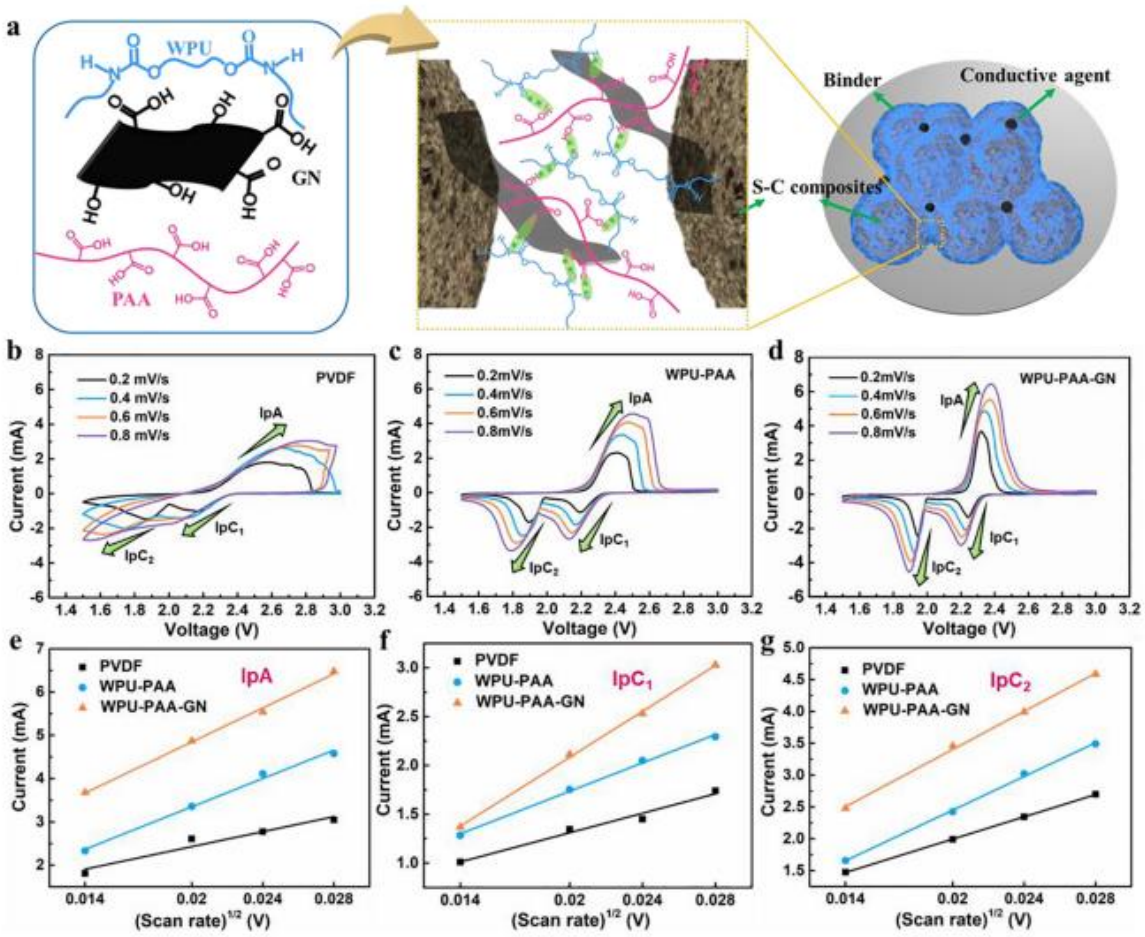


**Fig. 3**. (a) Schematic diagram of preparing sulfur cathode with WPU-PAA-GN composite binder. CV curves of Li-S batteries with (b) PVDF, (c) WPU-PAA, and (d) WPU-PAA-GN binders at different scan rates. Linear fits of CV peak current dependences based on the scan rate of Li-S batteries with (e) PVDF, (f) WPU-PAA, and (g) WPU-PAA-GN binders.

When the stretch-recovery cycles were performed at 50% and 100% strain limits, both samples showed a typical stretch-recovery curve with hysteresis loop, while the introduction of GN significantly increased the strength **[62,63].**

As shown in **Fig. 2**c and f, in order to analyze the influence of the cycle numbers on the stretch-recovery behavior of WPU-PAA and WPU-PAA-GN, we further calculated the plastic deformation (irreversible deformation) and energy loss (the area of hysteresis loop). For two samples, their plastic deformation and energy loss showed a large value in the first cycle, which indicated that there was a certain residual stress in the fresh formed film. However, with the progress of stretch-recovery, the composites tend to be stable. This phenomenon showed that the rigid flexible cross-linked network structure formed by intermolecular hydrogen bonding can have good structural stability in the process of charging and discharging, which was conducive to adapt to the volume change of sulfur. What's more, **Fig. 2**d showed the excellent resilience of WPU-PAA-GN film.

In addition, in order to evaluate the effect of different binders on the capture of lithium polysulfides (LiPSs), a static adsorption-barrier experiment was carried out in an H-type reactor. As shown in **Fig. 2**g-i, the left chamber is 0.05 M $Li_2S_6$-DOL/DME (1:1, V/V) solution, the right chamber is the same solution without $Li_2S_6$, and the replaceable separators in the middle are PVDF, WPU-PAA, and WPU-PAA-GN films, respectively. After 24 h, due to the weak interaction between the PVDF and the LiPSs **[64]**, $Li_2S_6$ in the left chamber had crossed the PVDF film and entered the right chamber. In WPU-PAA and WPU-PAA-GN reactors, the existence of abundant polar functional groups (carbamate and carboxyl) had strong chemical trapping effect on LiPSs, and the color of left chambers were obviously lighter. However, it is worth noting that WPU-PAA-GN can physically shield LiPSs due to the introduction of GN, so it has a better barrier effect on LiPSs. After 24 h, unlike WPU-PAA, which had slowly started to spread to the right chamber, the solution in the right chamber of WPU-PAA-GN was still clear. Therefore, WPU-PAA-GN binder is expected to absorb LiPSs in the process of charging and discharging, at the same time, to block LiPSs loss and reduce capacity loss **[65]**.

In order to study the application effect of WPU-PAA-GN binder in sulfur cathode, firstly, S/C composite materials were prepared by ball milling of sulfur and super P. XRD **(Fig. S8**a) patterns and Raman (**Fig. S8**b) spectra confirmed the existence of elemental sulfur in the S/C composite. FE-SEM image (Fig. S8c) showed that the sulfur and super P were evenly dispersed in the S/C composite. In addition, TGA curve (**Fig. S8**d) showed that the sulfur content in the S/C composite was about 75 wt%. After that, the S/C composite, conductive agent and binder were uniformly mixed and coated on the aluminum foil with a mass ratio of 8:1:1 to prepare the sulfur cathode. **Fig. 3**a vividly expressed that the WPU-PAA-GN binder can form an interwoven elastic network in S/C composite cathode.

In order to verify whether the synergistic effect of each component can promote the diffusion of lithium ion, CV curves (**Fig. 3**b-d) of three kinds of lithium sulfur batteries with different binders were measured at different scanning rates. With the increase of scanning rate, the oxidation peak (corresponding to the conversion of $Li_2S_2$/$Li_2S$ to long-chain LiPSs and eventually to $S_8$, peak A) shifted to the high voltage direction, and the reduction peaks (corresponding to the transformation of from $S_8$ to long-chain LiPSs, peak $C_1$, and then to insoluble $Li_2S_2$/ $Li_2S$, peak $C_2$) shifted to the low voltage direction. Compared with the PVDF-based cell, WPU-PAA and WPU-PAA-GN based cells can still show obvious oxidation and reduction peaks at a high scanning rate of 0.8 mV $s^{-1}$. From **Fig. 3**e-g, it can be seen that the peak current had a good linear relationship with the square root of scanning rate, which indicated that the reaction was controlled by diffusion. The higher the slope is, the higher the mass transfer efficiency is **[66]**. Therefore, WPU-PAA-GN based Li-S battery has the fastest reaction kinetics, which is consistent with the highest peak current results. Moreover, the diffusion coefficient of lithium ion ($D_{Li+}$) is evaluated by Randles-Sevcik formula **[67]**, $IP = 2.69 \times 10^5 n1.5AD^{0.5}_{Li+} CV^{0.5}$ where Ip is the peak current, n is the electron transfer number (n = 2), A is the area of the electrode ($cm^{-2}$), C is the concentration of lithium ion in electrolyte (0.001 mol $mL^{-1}$), and v is the scanning rate (V $s^{-1}$). The calculation results were listed in **Table S1**, which showed that the DLi+ in WPU-PAA-GN was

significantly higher than that of the other two binders. In the process of charging and discharging, the sulfur cathode will undergo serious polarization, and most of the reactions take place on the electrode surface, which is difficult to take place in the whole thickness **[68].** WPU-PAA-GN binder can promote the transport of lithium ion, and its application in sulfur cathode can reduce the polarization, which is very beneficial to improve the utilization of active materials.

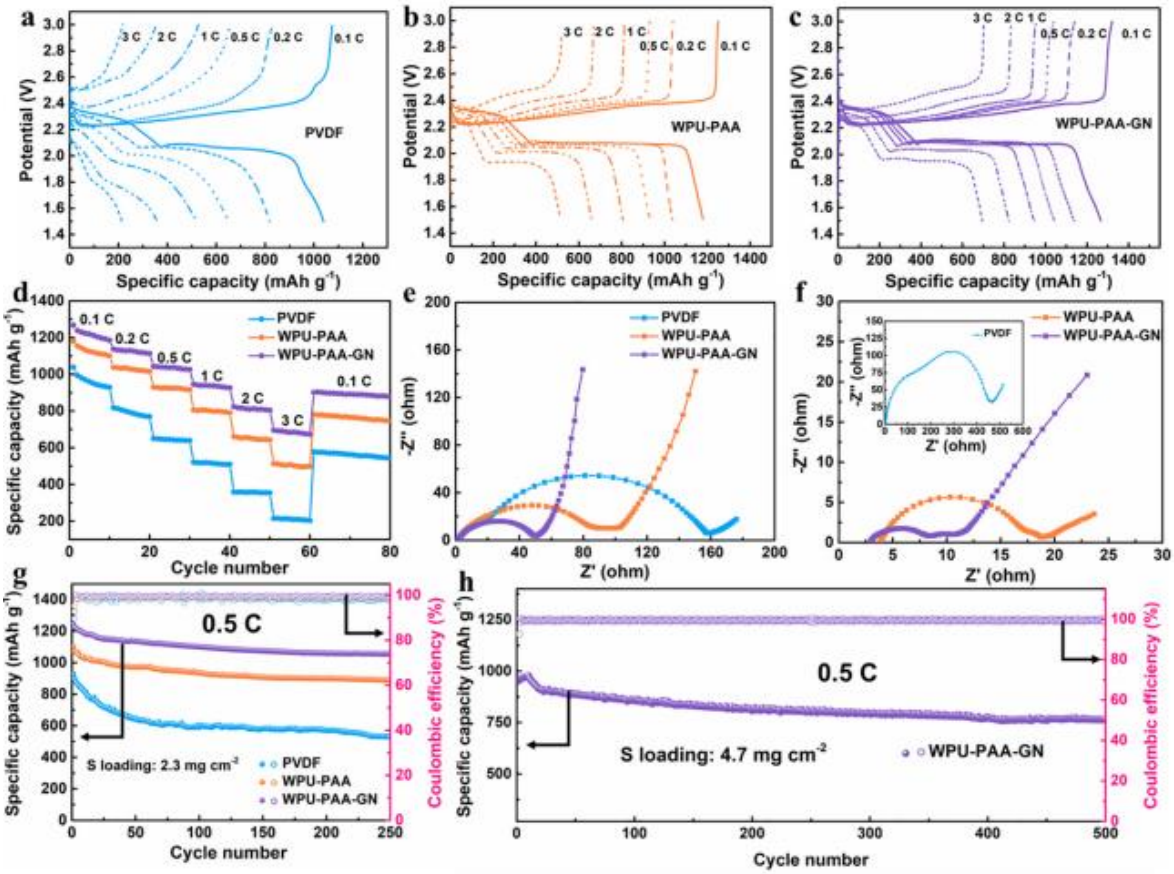


**Fig. 4.** Charge/discharge profiles of Li-S batteries with (a) PVDF, (b) WPU-PAA and (c) WPU-PAA-GN binders at various C-rates. (d) Rate capability, Electrochemical impedance spectroscopy tests (e) before cycling and (f) after 250 cycles, (g) Cycling performance at 0.5 C for Li-S batteries with PVDF, WPU-PAA and WPU-PAA-GN binders. (h) Long-term cycling performance of Li-S battery with WPU-PAA-GN binder at 0.5 C.

In order to evaluate the electrochemical properties of WPU-PAA-GN binder, five kinds of batteries with different binders were assembled and their electrochemical properties were compared. **Fig. 4**a, **S9**a, **S9**b, **4**b-c were the galvanostatic charge/discharge curves of PVDF, PAA, PAA-GN, WPU-PAA and WPU-PAA-GN under different current densities. All batteries had one charging platform and two discharging platforms under different current density, which represented the typical oxidation-reduction reaction of LiPSs and two-step reduction of **S8**. Obviously, the use of WPU-PAA-GN made the over potential of the battery smaller, indicating that it had better electrochemical reversibility. In addition, the initial discharge capacities of PVDF, PAA, PAA-GN, WPU-PAA and WPU-PAA-GN at 0.1 C were similar, which were 1038, 1088, 1150, 1179 and 1267 mAh $g^{-1}$, respectively. However, when the current density was further increased, the batteries with PAA-GN, WPU-PAA and WPU-PAA-GN binders still had stable discharge platform and high discharge capacity, while the Li-S battery with PVDF and PAA binders had significantly reduced discharge capacity, and the platform disappeared. Especially when the binder

was WPU-PAA-GN, it still had a specific capacity of 695 mAh $g^{-1}$ even at a high ratio of 3 C. This is consistent with the rate performance in **Fig. 4**d and **S9**c. Obviously, at high current density, the capacity attenuation of Li-S battery using WPU-PAA-GN binder was small. This showed that even a small amount of graphene can form an excellent conductive network in the electrode, which makes the electrochemical reaction happen smoothly. This can be further proved by electrochemical impedance spectrum.

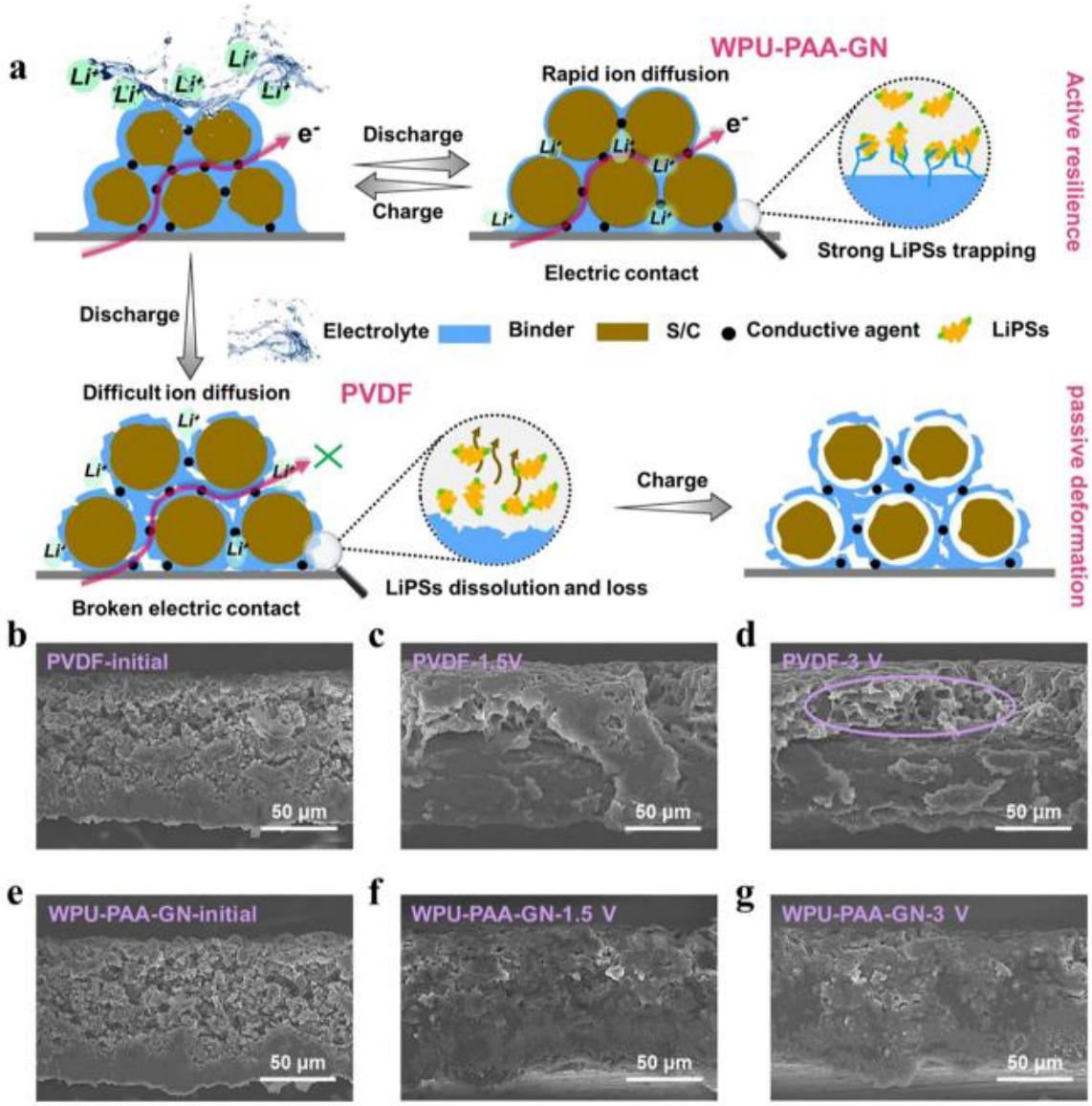


**Fig. 5.** (a) The mechanism of different binders on the dynamics-stability of Li-S batteries. The cross-section FE-SEM images of the cathode using PVDF binder (b) initial state, (c) at the end of discharge (1.5 V), (d) at the end of charging (1.5 V). The cross-section FE-SEM images of the cathode using WPU-PAA-GN binder (e) initial state, (f) at the end of discharge (1.5 V), (g) 3 V at the end of charging (3 V).

As shown in **Fig. 4**e, the charge-transfer resistances (50 Ω, 100 Ω) of sulfur cathode using WPU-PAA and WPU-PAA-GN were significantly lower than that of PVDF binder (159Ω). After 250 cycles, as shown in **Fig. 4**f, the bulk resistance of all three cells increased, and the charge transfer resistance using PVDF binder further increased to 465 Ω, but the charge transfer resistance of WPU-PAA and WPU-PAA-GN

cells decreased (11 Ω, 19 Ω). This may be attributed to the high ionic and electronic conductivity of the sulfur cathode and the adsorption capacity of rich polar functional groups, which inhibit the accumulation of insoluble LiPSs and improve the reversibility of the electrochemical reaction. With the increase of the cycle numbers, the transport of lithium ions becomes easier, which corresponds to the high rate performance.

**Fig. 4**g and S9d were the cycle performance of PVDF, PAA, PAA-GN, WPU-PAA and WPU-PAA-GN based batteries under the current density of 0.5 C and the sulfur loading was 2.3 mg $cm^{-2}$. The initial discharge capacities were 927, 1035, 1107, 1100 and 1243 mAh $g^{-1}$, respectively. After 250 cycles, the capacity retention of WPU-PAA and WPU-PAA-GN batteries were 80% and 85%, respectively, with an average attenuation of 0.08% and 0.06% per cycle. However, the capacity retention rate of PVDF, PAA, and PAA-GN battery was only 57%, 64% and 69%, and the average attenuation per cycle was as high as 0.17%, 0.14% and 0.12%. As shown in **Fig. 4**h, when the sulfur loading was further increased to 4.7 mg $cm^{-2}$, the initial discharge capacity reached 952 mAh g-1 at 0.5 C. At the beginning, the curve has a slow rising area, which may be due to the increase of the load made the electrode thicker and the electrolyte needed time to penetrate. After 500 cycles, it still had a specific capacity of 767 mAh $g^{-1}$ and the capacity retention rate of WPU-PAA-GN battery reached 81%. This showed that the use of WPU-PAA-GN binder enabled the battery to maintain better stability even under high sulfur loading. In addition, as shown in **Fig. S10**, the charge discharge curves under different cycles further illustrate the reversibility of the WPU-PAA-GN battery.

**Fig. 5**a vividly reveals the mechanism of the influence on the dynamics-stability of batteries by using of PVDF and WPU-PAA-GN binders. During charging and discharging, the sulfur active materials receive electrons from the conductive agent. At the same time, lithium ions are captured from the electrolyte, and the oxidation-reduction of sulfide is completed in the process. If the traditional PVDF binder is used, after the discharge is completed, S8 is converted to $Li_2S/Li_2S_2$, and the volume expansion is about 80%. However, PVDF has almost no elongation at break, so it cannot adapt to such volume deformation. This will lead to the separation of the conductive agent that originally adhered to the surface of the active materials, and the electronic path will become intermittent, accompanied by a large amount of dissolution and loss of LiPSs. Continue charging, at this time, $\mathbf{Li_2S/Li_2S_2}$ is converted to S8, and the volume is reduced. There is no way to follow the deformation of the PVDF binder so that the active material and the conductive agent are overhead, and ultimately reduce the cycle life of the battery. On the contrary, in WPU-PAA-GN binder, the high elasticity of WPU can meet the demand of volume expansion. The formation of WPU-PAA cross-linked network endows the binder with excellent resilience, so that it can deform along with the S/C composite. In addition, although the content of GN is only 1 wt%, the performance and cycle life of the battery have been significantly improved because the evenly distributed GN not only acts as the electron transport channel, but also provides a large area of active sites for the redox reaction. The rich polar groups on WPU-PAA-GN can realize the strong chemical capture of LiPSs like handles, which greatly reduces the loss of active materials.

In order to further confirm the above mechanism, FE-SEM images at different potentials were tested. As can be seen in **Fig. 5**c and f, at the end of discharge (1.5 V), there was a large amount of lithium sulfide deposition on the sulfur cathode, and the electrodes thickness were increased compared with that at the initial state (**Fig. 5**b and e). However, compared with the cathode using PVDF binder, the cathode using WPU-PAA-GN binder was much smoother. This is due to the inelasticity of PVDF, which belongs to passive deformation in the process of sulfur volume change. WPU-PAA-GN has excellent resilience and high strength. It belongs to active resilience in the process of sulfur volume change, and has a certain binding effect on volume expansion. When charging to 3 V, it can be seen from **Fig. 5**d and g that the cathode using PVDF binder not only had no significant change in thickness, but also had

a large area of honeycomb holes. The cathode using WPU-PAA-GN binder had basically returned to its original state. What's more, after 250 cycles, the FE-SEM images of Li anode were shown in **Fig. S11**. Compared with PVDF **Fig. S11**a and **11**b, there was no obvious corrosion layer in cross-section **Fig. S11**c of Li anode using WPU-PAA-GN binder, and the surface **Fig. S1**1d was relatively flat. This proves that the high resilience binder is very important for maintaining the stability of electrode structure. It can effectively improve the performance and life of lithium sulfur battery by giving the multiple functions for capturing LiPSs and providing conductive path.

## 4. Conclusions

In summary, a novel multifunctional WPU-PAA-GN composite binder with high resilience, strong capture and high conductivity was prepared by simple in-situ blending. By optimizing the amount of each component, the double hydrogen bond network structure was formed to alleviate the volume change during the charging and discharging process of lithium-sulfur batteries. Abundant polar groups can realize the strong chemical capture of LiPSs, and the physical shielding effect of easily dispersed graphene can effectively inhibit the shuttle effect. As a result, the assembled lithium sulfur battery shows excellent cycle stability (81% after 500 cycles at 0.5 C) and rate capacity (695 mAh $g^{-1}$ at high rate of 3 C).

## Appendix A. Supplementary data

Supplementary data to this article can be found online at **https:// doi.org/10.1016/j.cej.2020.124404.**

## References

[1] M. Armand, J.M. Tarascon, Building better batteries, Nature 451 (2008) 652-657.

[2] B. Dunn, H. Kamath, J.M. Tarascon, Electrical energy storage for the grid: a battery of choices, Science 334 (2011) 928-935.

[3] X.L. Ji, K.T. Lee, L.F. Nazar, A highly ordered nanostructured carbon-sulphur cathode for lithium-sulphur batteries, Nat. Mater. 8 (2009) 500-506.

[4] S. Urbonaite, T. Poux, P. Novák, Progress towards commercially viable Li-S battery cells, Adv. Energy Mater. 5 (2015) 1500118-1500137.

[5] X.Y. Zhou, Q.C. Liao, T. Bai, J. Yang, Nitrogen-doped microporous carbon from polyaspartic acid bonding separator for high performance lithium-sulfur batteries, J. Electroanal. Chem. 791 (2017) 167-174.

[6] L.L. Fan, M. Li, X.F. Li, W. Xiao, Z.W. Chen, J. Lu, Interlayer material selection for lithium-sulfur batteries, Joule 2 (2019) 361-386.

[7] X. Zhang, H. Xie, C.S. Kim, K. Zaghib, A. Mauger, C.M. Julien, Advances in lithium-sulfur batteries, Mater. Sci. Eng. R-Rep. 121 (2017) 1-29.

[8] T. Li, X. Bai, U. Gulzar, Y.J. Bai, C. Capiglia, W. Deng, X. Zhou, Z. Liu, Z. Feng, R. Proietti Zaccaria, A comprehensive understanding of lithium-sulfur battery technology, Adv. Funct. Mater. 29 (2019) 1901730.

[9] X. Lu, Q. Zhang, J. Wang, S. Chen, J. Ge, Z. Liu, L. Wang, H. Ding, D. Gong, H. Yang, X. Yu, J. Zhu, B. Lu, High performance bimetal sulfides for lithium-sulfur batteries, Chem. Eng. J. 358 (2019) 955-961.

[10] N. Deng, Y. Liu, Q.X. Li, J. Yan, L.T. Zhang, L.Y. Wang, Y.F. Zhang, B. Cheng, W.W. Lei, W.M. Kang, Functional double-layer membrane as separator for lithium-sulfur battery with strong catalytic conversion and excellent polysulfide-blocking, Chem. Eng. J. 382 (2019) 122918.

[11] Z.W. Zhang, H.J. Peng, M. Zhao, J.Q. Huang, Lithium-sulfur batteries: hetero-geneous/homogeneous mediators for high-energy-density lithium-sulfur batteries: progress and prospects, Adv. Funct. Mater. 28 (2018) 1707536.

[12] M. Wild, L. O'Neill, T. Zhang, R. Purkayastha, G. Minton, M. Marinescu, G.J. Offer, Lithium sulfur batteries, a mechanistic review, Energy Environ. Sci. 8 (2015) 3477-3494.

[13] D. Zheng, X.R. Zhang, J.K. Wang, D.Y. Qu, X.Q. Yang, D.Y. Qu, Reduction mechanism of sulfur in lithium-sulfur battery: from elemental sulfur to polysulfide, J. Power Sources 301 (2016) 312-316.

[14] Z.Y. Deng, L. Sun, Y. Sun, C.H. Luo, Q. Zhao, K.P. Yan, The phase transfer effect of sulfur in lithium-sulfur batteries, RSC Adv. 9 (2019) 32826-32832.

[15] M. Arslan, B. Kiskan, E.C. Cengiz, R. Demir Cakan, Y. Yagci, Inverse vulcanization of bismaleimide and divinylbenzene by elemental sulfur for lithium sulfur batteries, Eur. Polym. J. 80 (2016) 70-77.

[16] P.P.R.M.L. Harks, C.B. Robledo, T.W. Verhallen, P.H.L. Notten, F.M. Mulder, The significance of elemental sulfur dissolution in liquid electrolyte lithium sulfur batteries, Adv. Energy Mater. 7 (2017) 1601635.

[17] Y.C. Hao, D.B. Xiong, W. Liu, L.L. Fan, D.J. Li, X.F. Li, Controllably designed “viceelectrode” interlayers harvesting high performance lithium sulfur batteries, ACS Appl. Mater. Interfaces 46 (2017) 40273-40280.

[18] M. Zhao, H.J. Peng, Z.W. Zhang, B.Q. Li, X. Chen, J. Xie, X. Chen, J.Y. Wei, Q. Zhang, J.Q. Huang, Activating inert metallic compounds for high-rate lithium-sulfur batteries through in situ etching of extrinsic metal, Angew. Chem. Int. Ed. 58 (2019) 3779-3783.

[19] Z. Li, B.Y. Guan, J.T. Zhang, X.W. Lou, A Compact nanoconfined sulfur cathode for high-performance lithium-sulfur batteries, Joule 1 (2017) 576-587.

[20] Z. Zeng, W. Li, Q. Wang, X. Liu, Programmed design of a lithium-sulfur battery cathode by integrating functional units, Adv. Sci. 6 (2019) 1900711.

[21] W.C. Ren, W. Ma, S.F. Zhang, B.T. Tang, Recent advances in shuttle effect inhibition for lithium sulfur batteries, Energy Storage Mater. 23 (2019) 707-732.

[22] Z.F. Chen, X.D. Lin, H. Xia, Y.H. Hong, X.Y. Liu, S. Cai, J.N. Duan, J.J. Yang, Z.Y. Zhou, J.K. Chang, M.S. Zheng, Q.F. Dong, A functionalized membrane for lithium-oxygen batteries to suppress the shuttle effect of redox mediators, J. Mater. Chem. A 7 (2019) 14260-14270.

[23] H. Yuan, H.J. Peng, B.Q. Li, J. Xie, L. Kong, M. Zhao, X. Chen, J.Q. Huang, Q. Zhang, Conductive and catalytic triple-phase interfaces enabling uniform nucleation in high-rate lithium-sulfur batteries, Adv. Energy Mater. 9 (2019) 1802768.

[24] X.X. Peng, Y.Q. Lu, L.L. Zhou, T. Sheng, S.Y. Shen, H.G. Liao, L. Huang, J.T. Li, S.G. Sun, Graphitized porous carbon materials with high sulfur loading for lithium-sulfur batteries, Nano Energy 32 (2017) 503-510.

[25] H.J. Peng, J.Q. Huang, X.B. Cheng, Q. Zhang, Lithium-sulfur batteries: review on high-loading and high-energy lithium-sulfur batterie, Adv. Energy Mater. 7 (2017) 1770141.

[26] J. Kim, D. Byun, H.S. Kim, W. Choi, S.O. Kim, Surface-modified PVdF-derived hierarchical mesoporous carbon matrix for high sulfur loading cathode in lithium-sulfur batteries, J. Power Sources 427 (2019) 165-173.

[27] X. Huang, K. Zhang, B. Luo, H. Hu, D. Sun, S. Wang, Y. Hu, T. Lin, Z. Jia, L. Wang, Polyethylenimine expanded graphite oxide enables high sulfur loading and longterm stability of lithium-sulfur batteries, Small 15 (2019) 1804578.

[28] X. Chen, L.X. Yuan, Z.X. Hao, X.X. Liu, J.W. Xiang, Z.R. Zhang, Y.H. Huang, J. Xie, Freestanding Mn3O4@CNF/S paper cathodes with high sulfur loading for lithium-sulfur batteries, ACS Appl. Mater. Interfaces 10 (2018) 13406-13412.

[29] X.J. Liu, T. Qian, J. Liu, J.H. Tian, L. Zhang, C.L. Yan, Greatly improved conductivity of double-chain polymer network binder for high sulfur loading lithium-sulfur batteries with a low electrolyte/sulfur ratio, Small 14 (2018) 1801536.

[30] P. Han, S.H. Chung, C.H. Chang, A. Manthiram, Bifunctional binder with nucleophilic lithium polysulfide immobilization ability for high-loading, high-thickness cathodes in lithium-sulfur batteries, ACS Appl. Mater. Interfaces 11 (2019) 17393-17399.

[31] Y.P. Li, T.Y. Jiang, H. Yang, D. Lei, X.Y. Deng, C. Hao, F.X. Zhang, J.L. Guo, A heterostuctured Co3S4/MnS nanotube array as a catalytic sulfur host for lithium-sulfur batteries, Electrochim. Acta 330 (2019) 135311.

[32] Y. Zuo, R.L. Liu, X.C. Zhang, R. Nadimicherla, J. Huang, Y.H. Lu, S.H. Liu, D.C. Wu, R.W. Fu, A new supramolecular binder strongly enhancing the electrochemistry performance for lithium-sulfur batteries, Chem. Commun. 55 (2019) 13924-13927.

[33] H. Yuan, J.Q. Huang, H.J. Peng, M.M. Titirici, R. Xiang, R.J. Chen, Q.B. Liu, Q. Zhang, A review of functional binders in lithium-sulfur batteries, Adv. Energy Mater. 8 (2018) 1802107.

[34] M. Ling, L. Zhang, T.Y. Zheng, J. Feng, J.H. Guo, L.Q. Mai, G. Liu, Nucleophilic substitution between polysulfides and binders unexpectedly stabilizing lithium sulfur battery, Nano Energy 38 (2017) 82-90.

[35] C.A. Yang, Q.K. Du, Z.H. Li, M. Ling, X.Y. Song, V. Battaglia, X.B. Chen, G. Liu, In-situ covalent bonding of polysulfides with electrode binders in operando for lithium-sulfur batteries, J. Power Sources 402 (2018) 1-6.

[36] L. Wang, Z.H. Dong, D. Wang, F.X. Zhang, J. Jin, Covalent bond glued sulfur nanosheet-based cathode integration for long-cycle-life Li-S batteries, Nano Letters 13 (2013) 6244-6250.

[37] J. Liao, J. Wang, Z. Liu, Z. Ye, Polar Benzimidazole-containing (sulfonated) poly (arylene ether ketone)s as bifunctional binders for lithium-sulfur battery cathodes with high sulfur loadings, ACS Appl. Energy Mater. 2 (2019) 6732-6740.

[38] Z.A. Zhang, W.Z. Bao, H. Lu, M. Jia, K.Y. Xie, Y.Q. Lai, J. Li, Water-soluble polyacrylic acid as a binder for sulfur cathode in lithium-sulfur battery, ECS Electrochem. Lett. 1 (2012) A34-A37.

[39] G.Y. Xu, Q.B. Yan, A. Kushima, X.G. Zhang, J. Pan, J. Li, Conductive graphene oxide-polyacrylic acid (GOPAA) binder for lithium-sulfur battery, Nano Energy 31 (2017) 568-574.

[40] X.W. Fu, L. Scudiero, W.H. Zhong, A robust and ion-conductive protein-based binder enabling strong polysulfide anchoring for high-energy lithium-sulfur batteries, J. Mater. Chem. A 7 (2019) 1835-1848.

[41] G.R. Li, M. Ling, Y.F. Ye, Z.P. Li, J.H. Guo, Y.F. Yao, J.F. Zhu, Z. Lin, S.Q. Zhang, Acacia senegal-inspired bifunctional binder for longevity of lithium-sulfur batteries, Adv. Energy Mater. 5 (2015) 1500878.

[42] L. Zhang, M. Ling, J. Feng, G. Liu, J. Guo, Effective electrostatic confinement of polysulfides in lithium/sulfur batteries by a functional binder, Nano Energy 40 (2017) 559-565.

[43] J. Wang, Z. Yao, C.W. Monroe, J. Yang, Y. Nuli, Carbonyl-^-cyclodextrin as a novel binder for sulfur composite cathodes in rechargeable lithium batteries, Adv. Funct. Mater. 23 (2013) 1194-1201.

[44] H. Chen, M. Ling, L. Hencz, H.Y. Ling, G. Li, Z. Lin, G. Liu, S. Zhang, Exploring chemical, mechanical, and electrical functionalities of binders for advanced energy-storage devices, Chem. Rev. 118 (2018) 8936-8982.

[45] W. Chen, T. Qian, J. Xiong, N. Xu, X.J. Liu, J. Liu, J.Q. Zhou, X.W. Shen, T.Z. Yang, Y. Chen, C.L. Yan, A New type of multifunctional polar binder: toward practical application of high energy lithium sulfur batteries, Adv. Mater. 29 (2017) 1605160.

[46] M. Agostini, J.Y. Hwang, H.M. Kim, P. Bruni, S. Brutti, F. Croce, A. Matic, Y.K. Sun, Minimizing the electrolyte volume in Li-S batteries: a step forward to high gravimetric energy density, Adv. Energy Mater. 8 (2018) 1801560.

[47] W. Wahyudi, Z. Cao, P. Kumar, M.L. Li, Y.Q. Wu, M.N. Hedhili, T.D. Anthopoulos, L. Cavallo, L.J. Li, J. Ming, W. Wahyudi, Z. Cao, P. Kumar, M. Li, Y. Wu, M. N. Hedhili, T.D. Anthopoulos, L. Cavallo, L.J. Li, J. Ming, Phase inversion strategy to flexible freestanding electrode: critical coupling of binders and electrolytes for high performance Li-S battery, Adv. Funct. Mater. 28 (2018) 1802244.

[48] F. Wu, Y.S. Ye, R.J. Chen, T. Zhao, J. Qian, X.X. Zhang, L. Li, Q.M. Huang, X.D. Bai, Y. Cui, Gluing carbon black and sulfur at nanoscale: a polydopamine-based, “nanobinder” for double-shelled sulfur cathodes, Adv. Energy Mater. 7 (2017) 1601591.

[49] Z. Xu, J. Yang, T. Zhang, Y. Nuli, J. Wang, S.I. Hirano, Silicon microparticle anodes with self-healing multiple network binder, Joule 2 (2018) 950-961.

[50] J.Q. Zhou, H.Q. Ji, J. Liu, T. Qian, C.L. Yan, A new high ionic conductive gel polymer electrolyte enables highly stable quasi-solid-state lithium sulfur battery, Energy Storage Mater. 22 (2019) 256-264.

[51] Y.Y. Zhang, K. Li, H. Li, Y.Y. Peng, Y.H. Wang, J. Wang, J.B. Zhao, High sulfur loading lithium-sulfur batteries based on a upper current collector electrode with lithium-ion conductive polymers, J. Mater. Chem. A 5 (2017) 97-101.

[52] P. Xiao, F.X. Bu, G.H. Yang, Y. Zhang, Y.X. Xu, Integration of graphene, nano sulfur, and conducting polymer into compact, flexible lithium-sulfur battery cathodes with ultrahigh volumetric capacity and superior cycling stability for foldable devices, Adv. Mater. 29 (2017) 1703324.

[53] A.B. Puthirath, A. Baburaj, K. Kato, D. Salpekar, N. Chakingal, Y. Cao, G. Babu, P. M. Ajayan, High sulfur content multifunctional conducting polymer composite electrodes for stable Li-S battery, Electrochim. Acta 306 (2019) 489-497.

[54] M.Y. Wang, X.H. Xia, Y. Zhong, J.B. Wu, R.C. Xu, Z.J. Yao, D.H. Wang, W.J. Tang, X. L. Wang, J.P. Tu, Porous carbon hosts for lithium-sulfur batteries, Chem.-Eur. J. 25 (2019) 3710-3725.

[55] R.P. Fang, K. Chen, L.C. Yin, Z.H. Sun, F. Li, H.M. Cheng, Lithium batteries: the regulating role of carbon nanotubes and graphene in lithium-ion and lithium-sulfur batteries, Adv. Mater. 31 (2019) 1970066.

[56] Y.Z. Wang, M. Li, L.C. Xu, T.Y. Tang, Z. Ali, X.X. Huang, Y.L. Hou, S.Q. Zhang, Polar and conductive iron carbide@N-doped porous carbon nanosheets as a sulfur host for high performance lithium sulfur batteries, Chem. Eng. J. 358 (2019) 962-968.

[57] C. Milroy, A. Manthiram, An elastic, conductive, an elastic, conductive, electroactive nanocomposite binder for flexible sulfur cathodes in lithium-sulfur batteries, Adv. Mater. 28 (2016) 9744-9751.

[58] M.J. Lacey, V. Osterlund, A. Bergfelt, F. Jeschull, T. Bowden, D. Brandell, A robust, water-based, functional binder framework for high-energy lithium-sulfur batteries, Chemsuschem 10 (2017) 2758-2766.

[59A.L. Monaca, F.D. Giorgio, F. Soavi, G. Tarquini, M.D. Carli, P.P. Prosini, C. Arbizzani, Cover feature: 1,3-dioxolane: a strategy to improve electrode interfaces in lithium ion and lithium-sulfur batteries, ChemElectroChem 5 (2018) 1243.

[60] M.Q. Sun, G.C. Wang, X.W. Li, C.Z. Li, Irradiation preparation of reduced graphene oxide/carbon nanotube composites for high-performance supercapacitors, J. Power Sources 245 (2014) 436-444.

[61] S.J. Kim, Y.K. Jelong, Y. Wang, H. Lee, J.W. Choi, A “Sticky” mucin-inspired DNA-polysaccharide binder for silicon and silicon-graphite blended anodes in lithium-ion batteries, Adv. Mater. 30 (2018) 1707594.

[62] S.H. Choi, T.W. Kwon, A. Coskun, J. Wook Choi, Highly elastic binders integrating polyrotaxanes for silicon microparticle anodes in lithium ion batteries, Science 357 (2017)279-283.

[63] C.Y. Chen, H.J. Peng, T.Z. Hou, P.Y. Zhai, B.Q. Li, C. Tang, W. Zhu, J.Q. Huang, Q. Zhang, A Quinonoid-imine-enriched nanostructured polymer mediator for lithium-sulfur batteries, Adv. Mater. 29 (2017) 1606802.

[64] H.Q. Wang, V. Sencadas, G.P. Gao, H. Gao, A.J. Du, H.K. Liu, Z.P. Guo, Strong affinity of polysulfide intermediates to multi-functional binder for practical application in lithium-sulfur batteries, Nano Energy 26 (2016) 722-728.

[65] N.N. Hu, X.S. Lv, Y. Dai, L.L. Fan, D.B. Xiong, X.F. Li, A SnO2/reduced graphene oxide interlayer mitigating shuttle effect of Li-S batteries, ACS Appl. Mater. Interfaces 10 (2018) 18665-18674.

[66] N. Akhtar, H.Y. Shao, F. Ai, Y.P. Guan, Q.F. Peng, H. Zhang, W.K. Wang, A.B. Wang, B.Y. Jiang, Y.Q. Huang, Gelatin-polyethylenimine composite as a functional binder for highly stable lithium-sulfur batteries, Electrochim. Acta 282 (2018) 758-766.

[67] T.Y. Lei, W. Chen, W.Q. Lv, J.W. Huang, J. Zhu, J.W. Chu, C.Y. Yan, C.Y. Wu, Y. C. Yan, W.D. He, J. Xiong, Y.R. Li, C.L. Yan, J.B. Goodenough, X.F. Duan, Inhibiting polysulfide shuttling with a graphene composite separator for highly robust lithium-sulfur batteries, Joule 2 (2018) 2091-2104.

[68] W.L. Wu, J. Pu, J. Wang, Z.H. Shen, H.Y. Tang, Z.T. Deng, X.Y. Tao, F. Pan, H.G. Zhang, Biomimetic bipolar microcapsules derived from Staphylococcus aureus for enhanced properties of lithium-sulfur battery cathodes, Adv. Energy Mater. 8 (2018) 1702373.